

THE INFLUENCE OF MOISTURE CONTENT ON THE NONLINEAR CONSTITUTIVE BEHAVIOR OF CELLULOSIC MATERIALS

K. C. Yeh
Graduate Student
Department of Mechanical Engineering
Auburn University
Auburn, AL 36849-5341
U.S.A.

J. M. Considine
Research General Engineer
U. S. D. A. Forest Products Laboratory
One Gifford Pinchot Drive
Madison, WI 53705-2398
U.S.A.

J. C. Suhling
Associate Professor
Department of Mechanical Engineering
Auburn University
Auburn, AL 36849-5341
U.S.A.

ABSTRACT

In this project, the effects of moisture on the mechanical behavior of paperboard has been investigated. In particular, experiments under controlled environmental conditions have been performed to determine the effects of moisture content on the MD and CD initial elastic moduli, the Poisson's ratios, the initial shear modulus, and the shapes of the MD and CD uniaxial stress-strain curves. These results were then utilized to calculate the input parameters to a set of biaxial nonlinear elastic stress-strain relations for paperboard. The moisture dependence of the material constants and of the strain energy density function utilized within the nonlinear model have been determined.

INTRODUCTION

Paper materials tend to exhibit nonlinear mechanical behavior which is affected significantly by slight changes in the surrounding environmental conditions. In addition, most papers are capable of demonstrating every known rheological phenomenon. Current uses of paperboard provide several challenging problems in engineering mechanics. For example, paperboard is often utilized in structural applications such as corrugated containers where it is subjected to complicated biaxial stress states, including shear. At present, lack of accurate constitutive relations and reliable strength predictions under biaxial loading and variable environments hampers analysis of such problems. Therefore, it has been common practice in the paper industry to use trial and error, and empirical approaches for optimizing the designs of paperboard

products. This current lack of technology limits creative design improvements which could curtail the excess use of materials and energy.

A paper sheet is basically an assembly of discrete cellulose fibers bonded together into a complex network. The fibers tend to lie predominantly in the plane of the sheet. In addition, hydrodynamic forces present during sheet formation align the fibers primarily along the direction of web movement which is referred to as the machine direction (MD). Macroscopically, paper is an orthotropic solid. The in-plane directions of material symmetry are the machine direction (1-direction), and the in-plane direction perpendicular to MD which is called the cross-machine direction (CD or 2-direction).

As surveyed by Perkins [1] and Suhling [2], paper and paperboard have been modeled macroscopically using elastic, viscoelastic, and inelastic formulations. In a macromechanics or continuum approach, the material is presumed homogeneous and the effects of its micro-scale constituents are detected only as averaged apparent properties. Continuum models have the advantage of being applicable to complex structural design problems. For paper materials, continuum theories are typically established for a paper sheet or laminate viewed as three-dimensional orthotropic solid medium. The theory of linear orthotropic elasticity has been most often utilized to model the macroscopic behavior of paper. Since the mechanical behavior of most papers is highly nonlinear even at low strains, a linear elastic approach is unsuitable if high accuracy is desired.

There have been only a limited number of studies which have considered nonlinear elastic or elastic-plastic modeling of paper behavior. In the work of Thorpe [3], a tangential nonlinear elastic finite element analysis of a paper sheet in uniaxial extension was performed. An incremental approach was used to update the stiffness matrix. The utilized procedure calculated stiffness reductions based on experimentally measured uniaxial response. Such an approach allows no interaction (coupling) of the stresses in biaxial situations. This method is similar conceptually to earlier efforts for fiber-reinforced composites by Petit and Waddoups [4], and Sandhu [5]. A nonlinear finite element analysis of a spherical ball penetration test for paper has been performed by Ramasubramanian and Ko [6]. In their work, an elastic-plastic constitutive model was incorporated which included strain hardening patterned after measured uniaxial stress-strain data. In another recent investigation, Paetow and Gottsching [7] adopted a two parameter compliance model for the nonlinear stress-strain curve of paper. They then proposed an extension of this model for two-dimensional biaxial loading.

Another approach to modeling nonlinear elastic behavior is to use a so-called hyperelastic formulation. In such an approach, a strain energy density function must be found which accurately characterizes a material's nonlinear mechanical response. An advantage of this procedure is

that it is predictive in biaxial situations while allowing for stress interactions which are not directly dependent on the material's observed uniaxial response. Also, it can be shown [8] that all nonlinear elastic models consistent with the first law of thermodynamics must be obtainable from a strain energy density function. A strain energy approach for fiber-reinforced composites has been presented by Tsai and Hahn [9] for addressing nonlinear shear behavior. Conceptually similar nonlinear elastic analyses of composites using a complementary energy density function approach have been undertaken by Pindera and Herakovich [10], and Luo and Chou [11].

Suhling, et al. [12] have presented a total strain hyperelastic constitutive model for nonlinear orthotropic media and then applied it to paperboard. The nonlinear elastic constitutive equations presented were based on a special assumed form for strain energy density function suggested by Johnson and Urbanik [13]. Experimental data measured at Tappi standard conditions of 23°C and RH=50% were used to determine material constants and obtain the optimum functional form for the strain energy density function. Results from additional biaxial experiments were then utilized to validate the adequacy of the formulation. This nonlinear elastic formulation was also used in latter studies by Lin, et al. [14-15] to analyze the deformations, stresses, and strains of several paperboard structural configurations including the burst test. These studies showed that accurate correlations with experimental data could be obtained for complicated loadings and geometries using the nonlinear elastic theory, while poor agreement was obtained with linear elastic analyses.

It is well known that the most critical quantity influencing the characteristic mechanical response of a specific paper is its current and past history of moisture content. The moisture content or regain of an element of material is defined as the ratio of the difference between current weight and dry weight to the dry weight. For a particular sample of paper, the moisture content is determined predominately by the chemical and structural characteristics of its component fibers and the relative humidity (RH) of the surrounding atmosphere. It is also affected to a lesser degree by temperature, state of stress, and past histories of stress, temperature, and humidity. There has been relatively little research on the influence of moisture content on the mechanical behavior of paperboard. Also, the literature shows no experimental data or analytical results which relate the moisture content of a paperboard sheet to its constitutive response under biaxial loading.

In this project, the effects of moisture on the nonlinear biaxial mechanical response of paperboard has been investigated. In particular, experiments under controlled environmental conditions have been performed to determine the effects of moisture content on the MD and CD initial elastic moduli, the Poisson's ratios, the initial shear modulus, and the nonlinear shapes of the MD and CD uniaxial stress-strain curves. These results were then utilized to calculate the input parameters to the set of

biaxial nonlinear elastic (hyperelastic) stress-strain relations for paperboard presented by Suhling and co-workers [12]. The moisture dependence of the material constants and of the strain energy density function utilized within the model have been determined.

A NONLINEAR ELASTIC CONSTITUTIVE MODEL FOR PAPER

General Hyperelastic Formulation

An ideally elastic (hyperelastic or Green-elastic) material is defined as one for which a recoverable internal energy referred to as the strain energy exists. The strain energy density (per unit volume) is typically taken as a function of the strains. Such a material has a natural state to which the body will always return when the loading is released. No energy dissipation is allowed, so that the hyperelastic constitutive model is purely mechanical.

Using an energy balance equation obtained from the first law of thermodynamics and the above assumptions, it can be shown that the stress-strain relations in cartesian coordinates for a hyperelastic material are [8]

$$\sigma_{ij} = \frac{\partial W(\epsilon)}{\partial \epsilon_{ij}} \quad (\sigma_{ij} = \sigma_{ji}) \quad (1)$$

where σ_{ij} are the components of the familiar Cauchy stress tensor and W is the strain energy density function. In eqs. (1), the assumption of small deformation gradients has been made. For plane stress situations ($\sigma_{33} = \sigma_{13} = \sigma_{23} = 0$), eqs. (1) simplify to

$$\sigma_1 = \frac{\partial W}{\partial \epsilon_1}, \quad \sigma_2 = \frac{\partial W}{\partial \epsilon_2}, \quad \tau_{12} = \frac{\partial W}{\partial \gamma_{12}} \quad (2)$$

where $W = W(\epsilon_1, \epsilon_2, \gamma_{12})$ is now taken to be a function of the in-plane strains, and the conventional notations $\epsilon_1 = \epsilon_{11}$, $\epsilon_2 = \epsilon_{22}$, and $\gamma_{12} = 2\epsilon_{12}$ have been introduced.

For isotropic linear elastic materials, the appropriate strain energy density function for plane stress situations is

$$W = \frac{E}{2(1 - \nu^2)} (\epsilon_1 + \epsilon_2)^2 - \frac{E}{(1 + \nu)} (\epsilon_1 \epsilon_2 - \frac{\gamma_{12}^2}{4}) \quad (3)$$

where E is the elastic modulus and ν is the Poisson's ratio. For linear orthotropic elasticity, the correct strain energy density function for plane stress situations is

$$W = \frac{E_1}{2(1 - \nu_{12}\nu_{21})} (\epsilon_1^2 + \nu_{21}\epsilon_1\epsilon_2) + \quad (4)$$

$$\frac{E_2}{2(1 - \nu_{12}\nu_{21})} (\epsilon_2^2 + \nu_{12}\epsilon_1\epsilon_2) + \frac{1}{2} G_{12} \gamma_{12}^2$$

where E_1 and E_2 are elastic moduli, ν_{12} and ν_{21} are Poisson's ratios, G_{12} is the shear modulus, and the in-plane strains ϵ_1 , ϵ_2 , γ_{12} are now exclusively evaluated in an x_1 - x_2 coordinate system aligned along the directions of material symmetry. The familiar isotropic and orthotropic versions of plane stress Hooke's Law are obtained by

substituting eq. (3) and eq. (4) into eqs. (2), respectively.

Nonlinear Elastic Constitutive Model

The linear orthotropic strain energy density function given in eq. (4) can be rewritten in the form

$$W = \frac{\nu_{21} E_1}{2(1 - \nu_{12}\nu_{21})} e \quad (5)$$

where e is a positive definite effective strain measure given by

$$e = \frac{\epsilon_1^2}{\nu_{21}} + \frac{\epsilon_2^2}{\nu_{12}} + 2\epsilon_1\epsilon_2 + \frac{C}{4}\gamma_{12}^2 \quad (6)$$

Constant C in eq. (6) is related to the shear modulus

$$C = \frac{4(1 - \nu_{12}\nu_{21})}{\nu_{21}E_1} G_{12} \quad (7)$$

For nonlinear orthotropic media under plane stress conditions, a theory based on an assumed form for the strain energy density function has been presented by Suhling, et al. [12], and Johnson and Urbanik [13]. In these studies, it was assumed that a class of materials exists for which W can be expressed as a nonlinear function of the single variable e found in the linear orthotropic theory

$$W = W(e) \quad (8)$$

Substitution of eq. (8) into eqs. (2) leads to the stress-strain relations (plane stress) for the suggested nonlinear theory

$$\begin{aligned} \sigma_1 &= 2W'(e) \left[\frac{\epsilon_1}{\nu_{21}} + \epsilon_2 \right] \\ \sigma_2 &= 2W'(e) \left[\frac{\epsilon_2}{\nu_{12}} + \epsilon_1 \right] \\ \tau_{12} &= \frac{C}{2} W'(e) \gamma_{12} \end{aligned} \quad (9)$$

The material constants ν_{12} , ν_{21} , C and the functional form of the strain energy density derivative $W'(e)$ are to be determined from experimental data. These equations are for a coordinate system aligned with the directions of material symmetry.

It is often convenient to express eqs. (9) in matrix form

$$\begin{bmatrix} \sigma_1 \\ \sigma_2 \\ \tau_{12} \end{bmatrix} = 2W'(e) [Q_{ij}] \begin{bmatrix} \epsilon_1 \\ \epsilon_2 \\ \gamma_{12} \end{bmatrix} \quad (10)$$

where symmetric components Q_{ij} of the stiffness matrix are given by

$$Q_{11} = \frac{1}{\nu_{21}}, \quad Q_{12} = Q_{21} = 1, \quad Q_{22} = \frac{1}{\nu_{12}}, \quad (11)$$

$$Q_{33} = \frac{C}{4}, \quad Q_{13} = Q_{31} = Q_{23} = Q_{32} = 0$$

Equation (10) can be inverted to give

$$2W'(e) \begin{bmatrix} \epsilon_1 \\ \epsilon_2 \\ \gamma_{12} \end{bmatrix} = [S_{ij}] \begin{bmatrix} \sigma_1 \\ \sigma_2 \\ \tau_{12} \end{bmatrix} \quad (12)$$

where the compliance matrix $[S_{ij}]$ is the inverse of the stiffness matrix $[Q_{ij}]$. The compliance coefficients S_{ij} are given by

$$\begin{aligned} S_{11} &= \frac{\nu_{21}}{(1 - \nu_{12}\nu_{21})}, \quad S_{22} = \frac{\nu_{12}}{(1 - \nu_{12}\nu_{21})} \\ S_{12} = S_{21} &= \frac{-\nu_{12}\nu_{21}}{(1 - \nu_{12}\nu_{21})}, \quad S_{33} = \frac{4}{C} \\ S_{13} = S_{31} = S_{23} = S_{32} &= 0 \end{aligned} \quad (13)$$

It should be noted that in general, the strains can not be determined from the stresses using eq. (12). This is because the nonlinear function $W'(e)$ multiplies each of the strain components.

Nonlinear Theory - Uniaxial Loading

For uniaxial extension in the x_1 -direction ($\sigma_2 = \tau_{12} = 0$), eqs. (12) become

$$\begin{aligned} 2W'(e) \epsilon_1 &= S_{11} \sigma_1 \\ 2W'(e) \epsilon_2 &= S_{12} \sigma_1 \\ 2W'(e) \gamma_{12} &= 0 \end{aligned} \quad (14)$$

Algebraic manipulation of these expressions yields the following relationships:

$$\sigma_1(\epsilon_1) = 2W'(e) \left[\frac{1 - \nu_{12}\nu_{21}}{\nu_{21}} \right] \epsilon_1 \quad (15)$$

$$\epsilon_2 = -\nu_{12} \epsilon_1 \quad (16)$$

$$\gamma_{12} = 0 \quad (17)$$

Equation (16) demonstrates that the nonlinear theory predicts that parameter ν_{12} is a constant Poisson's ratio just as in the linear orthotropic theory.

The effective strain for this loading is simplified by substituting eqs. (16,17) into eq. (6)

$$e = \left[\frac{1 - \nu_{12}\nu_{21}}{\nu_{21}} \right] \epsilon_1^2 \quad (18)$$

Combining eqs. (15,18) by using a chain rule yields

$$\sigma_1(\epsilon_1) = \frac{dW}{de} \frac{de}{d\epsilon_1} \quad (19)$$

or

$$\sigma_1(\epsilon_1) = \frac{dW(\epsilon_1)}{d\epsilon_1} \quad (20)$$

Equation (20) can be integrated directly to obtain $W(\epsilon_1)$ when $\sigma_1(\epsilon_1)$ is represented by an experimentally determined empirical formula. Function $W(e)$ is obtained from this result by substituting

$$\epsilon_1 = \sqrt{\frac{\nu_{21}e}{1 - \nu_{12}\nu_{21}}} \quad (21)$$

Differentiation of eq. (15) with respect to ϵ_1 leads to an expression for the tangent modulus of the 1-direction uniaxial stress-strain curve

$$E_{T1}(\epsilon_1) = 4W''(e) \left[\frac{1 - \nu_{12}\nu_{21}}{\nu_{21}} \right]^2 \epsilon_1^2 + 2W'(e) \left[\frac{1 - \nu_{12}\nu_{21}}{\nu_{21}} \right] \quad (22)$$

From eq. (22), the initial (zero strain) elastic modulus is given by

$$E_1 = E_{T1}(0) = 2W'(0) \left[\frac{1 - \nu_{12}\nu_{21}}{\nu_{21}} \right] \quad (23)$$

Analogous results can be derived for uniaxial extension in the 2-direction. In this case, the relevant equations are

$$\sigma_2(\epsilon_2) = \frac{dW(\epsilon_2)}{d\epsilon_2} = 2W'(e) \left[\frac{1 - \nu_{12}\nu_{21}}{\nu_{12}} \right] \epsilon_2 \quad (24)$$

$$\epsilon_1 = -\nu_{21}\epsilon_2 \quad (25)$$

$$e = \left[\frac{1 - \nu_{12}\nu_{21}}{\nu_{12}} \right] \epsilon_2^2 \quad (26)$$

$$E_2 = 2W'(0) \left[\frac{1 - \nu_{12}\nu_{21}}{\nu_{12}} \right] \quad (27)$$

Equation (24) can also be integrated to determine function $W(e)$ if $\sigma_2(\epsilon_2)$ is represented by an experimentally determined empirical formula. Elimination of $W'(0)$ from eqs. (23,27) gives the relation

$$\nu_{12}E_2 = \nu_{21}E_1 \quad (28)$$

This is an extension of the familiar linear elastic formula since E_1 and E_2 are initial moduli in the nonlinear material model being considered.

The nonlinear constitutive theory predicts constant Poisson's ratios while allowing for nonlinear uniaxial stress-strain curves. Also, no normal-shear coupling is present with uniaxial testing in the directions of material symmetry. The paper experimental data measured by Suhling, et al. [12] at Tappi standard conditions have

demonstrated that these attributes are desirable in a nonlinear stress-strain model for paper. If these trends are found to be valid at other moisture levels, then there exists a high potential that the nonlinear stress-strain relations will accurately model paper elastic behavior over a wide range of moisture contents. Inelastic behavior can also be modeled if only loading situations are considered.

Nonlinear Theory - Pure Shear Loading

In the case of on-axis pure shear loading ($\sigma_1 = \sigma_2 = 0$), eqs. (9) simplify to

$$\epsilon_1 - \epsilon_2 = 0 \quad (29)$$

$$\tau_{12} = \frac{C}{2} W'(e) \gamma_{12} \quad (30)$$

The effective strain for this loading is evaluated by substituting eqs. (29) into eq. (6)

$$e = \frac{C}{4} \gamma_{12}^2 \quad (31)$$

A prediction for the instantaneous (tangent) shear modulus of the shear stress-strain curve is obtained through differentiation of eq. (30) with respect to γ_{12}

$$G_T(\gamma_{12}) = \frac{d\tau_{12}(\gamma_{12})}{d\gamma_{12}} = \frac{C^2}{4} W''(e) \gamma_{12}^2 + \frac{C}{2} W'(e) \quad (32)$$

The material constant C in the nonlinear theory can be related to the initial (zero strain) shear modulus by setting $\gamma_{12} = 0$ in eq. (32)

$$C = \frac{2G_{12}}{W'(0)} \quad (33)$$

Measurement of the Input Parameters to the Nonlinear Theory

The input parameters to the nonlinear theory are the three material constants ν_{12} , ν_{21} , C , and the functional form of the strain energy density function derivative $W'(e)$. These quantities should be determined using data obtained from experimental testing at various moisture levels. Once the dependence of the input parameters on moisture is found, the biaxial nonlinear elastic behavior of paper at various moisture contents can be predicted. Through use of the expressions presented above, the needed material characterization at a given moisture level can be completed using the data obtained from uniaxial tests in the 1- and 2-directions, and pure shear tests.

In the first step of the material characterization procedure, uniaxial extension tests in the 1- and 2-directions should be performed. In these experiments, the axial stress, axial strain, and transverse strain must all be monitored. The Poisson's ratios ν_{12} and ν_{21} can be evaluated using linear regression fits to the transverse strain vs. axial strain data. The functional form of strain energy density function $W(e)$ can then be found by

integrating an empirical representation of the uniaxial 1-direction stress-strain data using eq. (20) or by integrating an empirical representation of the uniaxial 2-direction stress-strain data using eq. (24). The values of the Poisson's ratios must be known before either of these integration procedures can be implemented. The derivative $W'(e)$ can be easily found by differentiating this result either analytically or numerically.

In the second step of the procedure, pure shear testing should be performed (such as torsion of cylindrical tubes). The initial shear modulus G_{12} can be determined from measurements of the initial slope of the shear stress-strain curves. Constant C can then be evaluated by substituting the value of G_{12} and the zero strain value of the strain energy density derivative into eq. (33).

MATERIAL CHARACTERIZATION AT VARIOUS MOISTURE LEVELS

In order to evaluate the input parameters to the nonlinear constitutive relations at different moisture levels, uniaxial extension tests and pure shear experiments have been conducted under controlled environmental conditions. All testing in this study was performed on 100% Lakes States softwood unbleached Kraft paper (basis weight 205 g/m², mass density 670 kg/m³). Experiments were performed in a specially constructed environmental chamber conditioned to different levels of relative humidity. Environmental conditions were adjusted in the chamber using a microcomputer-based feedback control system incorporating input from a humidity transducer and output to a flow control valve which mixed humid and dry air. Figure 1 shows a photograph of the chamber and the conditioning unit.

Characteristic Adsorption Curve

The environmental conditions for the various experiments were changed by adjusting the relative humidity of the surrounding air. All specimens for the mechanical tests were first preconditioned in a desiccant chamber for several days. Then before loading, they were placed in the chamber and allowed to adsorb moisture and equilibrate at the particular relative humidity level of the test being performed. The temperature for all experiments was maintained at a constant level of 23°C.

To relate the observed material test results to sheet moisture content, the characteristic moisture adsorption curve of the paper under consideration was measured according to TAPPI standard T 412 om-83. The samples for the adsorption measurements were preconditioned inside a desiccant chamber for several days to allow the paper to achieve sorption equilibrium at approximately 0% RH. Dry weight measurements were first done by heating the paper specimens inside an oven at a temperature of 105°C, placing them in a bottle of known weight, and then weighing the bottle and specimen. The

specimens were then removed from the bottle and placed on a sensitive scale in the environmental chamber. Specimen weights were recorded at relative humidity levels of 40%, 50%, 60%, 70%, 80%, 90%, 93%, 96%, and 98%. The samples were allowed to equilibrate for one hour at each RH level before the weight was recorded. At a given RH, the moisture content of each specimen was calculated from the recorded weight at that RH and the dry weight. Figure 2 shows the obtained relationship between the moisture content of the paper and the relative humidity of the surrounding air. Each data point represents the average of six specimens. The data plotted in Figure 2 is tabulated in Figure 3.

Uniaxial Extension Data

Uniaxial extension experiments were performed at relative humidity levels of 40%, 50%, 60%, 70%, 80%, 90%, and 95%. Between six and fifteen uniaxial tensile tests were performed in both the MD and CD at each specific RH level, and all specimens were loaded to failure. According to ASTM & TAPPI testing standards, the uniaxial specimens were prepared by cutting out 15.24 by 5.08 cm rectangular samples which were then cut into a dogbone shape. A pair of loading tabs were glued to the ends of the dogbone specimens using a hot melt adhesive. Figure 4 shows specimen assemblies before and after testing. As discussed above, all specimens were placed inside a desiccant chamber to allow the glue to dry thoroughly and to allow the paper to reach sorption equilibrium at a very low moisture level prior to testing. Just before testing, specimens were introduced into the environmental chamber and maintained at the desired RH for one hour before beginning an experiment.

All experiments were performed using a modified version of the vacuum restraint apparatus developed by Gunderson [16]. In this work, a pressure differential was not maintained across the specimen, and the restraint system was used primarily as a lateral support mechanism for the horizontally loaded specimens. The flat surface supporting the specimens was formed by the ends of an array of slender rods of circular cross-sectional area. The ends of rods touching the specimen were free to rotate as the specimen deformed. One significant advantage of the lateral support method is that one surface of the specimen is fully accessible for measurement of deformation and for observation of failure phenomena. A specially designed load frame was used to test the specimens within the environmental chamber. Figure 5 shows the entire uniaxial extension testing unit.

A PC-based data acquisition and control system was used to control the load frame motor speed and maintain a constant strain rate. The load frame was servo-driven so that it achieved a specified strain rate of 0.0015 sec⁻¹ independent of load magnitude. The quantities recorded during the uniaxial tests were axial extension, transverse contraction, and load. Two perpendicular extensometers were used to measure the extension and contraction as shown in Figure 5. A load cell attached to the load frame was utilized to monitor the load. In addition to

controlling the strain rate, the PC-based data acquisition system was also used to record the load and deformation signals from the extensometers and the load cell. Typical test durations varied from 10 to 40 seconds.

Figure 6 shows the obtained uniaxial MD and CD stress-strain curves at the seven different levels of relative humidity (moisture) considered. These curves clearly illustrate highly nonlinear mechanical behavior. Response is partially elastic into the nonlinear parts of the curves but not all the way to failure. The nonlinear stress-strain data shown in Figure 6 have been modeled accurately using a three parameter hyperbolic tangent empirical representation

$$\sigma(\epsilon) = C_1 \tanh(C_2 \epsilon) + C_3 \epsilon \quad (34)$$

This model was originally suggested by Andersson and Berklyto [17], and has later been adopted by several investigators. Differentiation of eq. (34) leads to an expression for the initial (zero strain) elastic modulus

$$E = C_1 C_2 + C_3 \quad (35)$$

Constants C_1 , C_2 , and C_3 were determined for the MD and CD test results at the different humidity levels by performing nonlinear regression analyses of eq. (34) through experimental data points from the tensile experimental curves in Figure 6. The commercially available program NREG77 was utilized on a IBM-PC compatible computer to perform the regression calculations. This numerical routine calculated the optimum coefficients which gave the best fit of the model to the data in the least-squares sense. For each testing orientation and moisture level, experimental data from all of the stress-strain curves were fit simultaneously in the regression analysis.

Figure 7 tabulates the calculated regression coefficients, and the initial elastic moduli evaluated with eq. (35). In Figure 8, the correlations of equation (34) with the uniaxial experimental curves are presented. In these plots, the thinner curves represent the experimental stress-strain data while the thick curves were obtained by using the hyperbolic tangent model and the calculated regression coefficients. At all moisture levels, the empirical model correlates extremely well with the experimental data. Figure 9 illustrates the observed variation of the initial elastic moduli E_1 and E_2 with moisture content. A pair of linear regression fits to this data have been included to demonstrate the approximate linear variation of the moduli. The exponential model suggested by Nissan [18] was also found to fit this data well.

The Poisson's ratios ν_{12} and ν_{21} were determined from the axial and transverse strain data measured during the uniaxial tests. Figures 10 and 11 contain plots of the experimental strain-strain data at different relative humidity levels for the MD and CD uniaxial extension tests, respectively. The shapes of these experimental strain-strain curves agree qualitatively with limited results for paper given previously by Brecht and Wanka [19], and Gottsching and Baumgarten [20]. The slopes of

the strain-strain curves for MD extension tests tend to increase monotonically with strain. However, the strain-strain curves for the CD extension tests were slightly "S" shaped where the slopes first decrease and then later increase. At all moisture levels, the observed strain-strain curves can be adequately approximated using straight line representations. Therefore, it is a reasonable engineering approximation to assume that the Poisson's ratios of paperboard are independent of strain.

A set of composite data was formed for each testing direction and moisture level by combining all of the data from the tests at a given set of conditions. For each of the 14 combined sets, a linear regression analysis was performed to find the best straight line fit to the experimental data points in the least-squares sense. The Poisson's ratio values were taken as the slopes of these optimum straight line fits to each combined data set. The values of the calculated Poisson's ratios are tabulated in Figure 12. Figure 13 contains plots of the Poisson's ratios versus moisture content. Both the values of ν_{12} and ν_{21} were observed to increase with increasing moisture level. This trend was also reported by Brecht and Wanka [19] using very limited data. In addition, the data measured in this investigation illustrate an approximate linear dependence of the Poisson's ratios with moisture content.

In linear orthotropic elasticity theory, the Poisson's ratios are to be evaluated for small strains. Separate small strain values of the Poisson's ratio were obtained by evaluating the slopes of the initial linear portions of the strain-strain curves. Initial values of ν_{12} were found by averaging the values of the slopes of the initial linear portions of the curves in Figure 10, and initial values of ν_{21} were found by averaging the values of the slopes of the initial linear portions of the curves in Figure 11. The calculated initial Poisson's ratios are tabulated in Figure 12, and Figure 14 shows the measured variation of the initial Poisson's ratios with moisture content. Only a slight variation of the small strain Poisson's ratios was observed. A similar result was also obtained by Baum, Brennan, and Habeger [21] using ultrasonic measurements.

Shear Modulus Data

Pure shear stress-strain curves for paperboard have been obtained at several moisture levels by subjecting specially fabricated cylindrical tube specimens to torsional loading. Initial shear moduli were evaluated from the initial slopes of the measured shear stress-strain curves. The torsion testing technique utilized here was a modified version of the method presented originally by Setterholm and co-workers [22]. The quantities measured during the experiments were the applied torque and the angle of twist. A picture of a specimen assembly in the torsion device is shown in Figure 15. The applied torque was obtained by using a load cell to measure the force transmitted by a torque arm attached to one of the loading heads. A new technique was used to measure the angle of twist continuously with an extensometer. The edges of the extensometer rested on aluminum rods

attached to plexiglas rings which engaged the paper specimen via pointed retaining pins. The output of this extensometer has been related to the relative angle of twist between the two rings by using trigonometry and the alternating series convergence theorem [23]. Sets of torque-twist data points were recorded by feeding the electrical signals from the extensometer and load cell into a PC-based data acquisition system. The shear stress and shear strain in a torsion specimen are related linearly to the torque and twist, respectively. Therefore, shear stress-strain data could be obtained easily with minor scale factor adjustments.

A total of fifty-four paper samples were tested with the improved version of the torsion apparatus. Six torsion tests were performed at relative humidity levels of 16%, 30%, 40%, 50%, 60%, 70%, 80%, 90%, and 95%. Figure 16 illustrates a typical measured shear stress-strain curve. A pure shear failure could not be obtained with present torsion apparatus because buckling occurred perpendicular to the maximum compressive stress (at an angle of 45° from the axis of the cylinder). The initial shear modulus for each experiment was obtained by applying a linear curve fit to the initial linear portion of the stress-strain curve. At each moisture level, the initial shear modulus was calculated by averaging the slopes for all tests at that humidity. The calculated average values of the initial shear moduli are tabulated in Figure 17. A plot of initial shear modulus versus moisture content is shown in Figure 18. The observed variation is approximately linear.

INPUT PARAMETERS TO THE NONLINEAR THEORY

As discussed previously, the input parameters to the nonlinear theory are the three material constants ν_{12} , ν_{21} , C , and the functional form of the strain energy density function derivative $W'(e)$. Each of these quantities have been evaluated for the paper material under consideration using the uniaxial and shear data presented in the last section. The results of these calculations are now discussed.

Poisson's Ratios

As discussed above, the Poisson's ratios ν_{12} and ν_{21} have been found as a function of moisture content. The obtained values are tabulated in Figure 12 and plotted in Figure 13. It is recommended that linear regression fits to the strain-strain curves over the entire strain range be used to find the Poisson's ratios needed for the nonlinear theory, and that initial (zero strain) values of the Poisson's ratios not be used. The greatest advantage of the nonlinear stress-strain relations is its ability to model mechanical behavior in situations where the strains are not small and nonlinear effects have occurred. Therefore, Poisson's ratios valid over a wide range of strain levels provide the best input to the nonlinear constitutive theory.

Strain Energy Density Function Derivative

Once the Poisson's ratios have been obtained, it is possible to find the functional form of the strain energy density function $W(e)$ using either eq. (20) or eq. (24). The experimental MD and CD uniaxial stress-strain data for paperboard presented earlier have been accurately represented at all levels of moisture by the three parameter hyperbolic tangent empirical model given in eq. (34). At a given moisture level, the stress-strain curves can then be modeled by the expressions

$$\sigma_1(\epsilon_1) = C_1^{MD} \tanh(C_2^{MD} \epsilon_1) + C_3^{MD} \epsilon_1 \quad (36)$$

$$\sigma_2(\epsilon_2) = C_1^{CD} \tanh(C_2^{CD} \epsilon_2) + C_3^{CD} \epsilon_2 \quad (37)$$

Calculated values of the MD and CD regression coefficients at various moisture contents have been tabulated in Figure 7.

An expression for the strain energy density function $W(\epsilon_1) = W_{MD}(\epsilon_1)$ can be obtained by substituting the MD hyperbolic tangent empirical model in eq. (36) into eq. (20), and performing the integration. Using eq. (21) to change variable ϵ_1 to e leads to

$$W_{MD}(e) = \frac{C_1^{MD}}{C_2^{MD}} \text{Log} \left[\cosh \left(C_2^{MD} \sqrt{\frac{\nu_{21}e}{1 - \nu_{12}\nu_{21}}} \right) \right] + \frac{C_3^{MD} \nu_{21}e}{2(1 - \nu_{12}\nu_{21})} \quad (38)$$

Performing an analogous calculation using the CD hyperbolic tangent empirical expression in eq. (37) and eqs. (24,26) yields another expression for the strain energy density function

$$W_{CD}(e) = \frac{C_1^{CD}}{C_2^{CD}} \text{Log} \left[\cosh \left(C_2^{CD} \sqrt{\frac{\nu_{12}e}{1 - \nu_{12}\nu_{21}}} \right) \right] + \frac{C_3^{CD} \nu_{12}e}{2(1 - \nu_{12}\nu_{21})} \quad (39)$$

The derivatives of the functions in eqs. (38,39) are

$$W'_{MD}(e) = \frac{C_1^{MD}}{2\sqrt{e}} \sqrt{\frac{\nu_{21}}{1 - \nu_{12}\nu_{21}}} \tanh \left(C_2^{MD} \sqrt{\frac{\nu_{21}e}{1 - \nu_{12}\nu_{21}}} \right) + \frac{C_3^{MD} \nu_{21}}{2(1 - \nu_{12}\nu_{21})} \quad (40)$$

$$W'_{CD}(e) = \frac{C_1^{CD}}{2\sqrt{e}} \sqrt{\frac{\nu_{12}}{1 - \nu_{12}\nu_{21}}} \tanh \left(C_2^{CD} \sqrt{\frac{\nu_{12}e}{1 - \nu_{12}\nu_{21}}} \right) + \frac{C_3^{CD} \nu_{12}}{2(1 - \nu_{12}\nu_{21})} \quad (41)$$

The biaxial stress-strain relations of the nonlinear orthotropic constitutive theory have been presented in eq.

(9). These expressions could be used with either the function $W'_{MD}(e)$ in eq. (40) or the function $W'_{CD}(e)$ in eq. (41) to characterize the nonlinear mechanical behavior of paperboard. Which of the two derivative expressions is more suitable depends on the type of accuracy required. If the strain energy density function derivative $W'_{MD}(e)$ is used, the nonlinear theory degenerates to eq. (36) for the case of MD uniaxial extension. That is, the theory matches the MD uniaxial experimental data in an optimum manner. Similarly, the nonlinear theory will match the CD uniaxial experimental data in an optimum manner by predicting the response in eq. (37) when the function $W'_{CD}(e)$ is utilized.

A detailed analysis using the available uniaxial data for paperboard has demonstrated that neither of the strain energy density function derivatives in eq. (40) or eq. (41) will allow the nonlinear constitutive theory to accurately predict both MD and CD uniaxial response at a given moisture level. Therefore, another expression for the strain energy density function derivative has been formulated. This "compromise" strain energy density function derivative $W'_{comp}(e)$ allows the nonlinear theory to correlate satisfactorily with both MD and CD uniaxial data. A formula for the compromise strain energy density function derivative can be established by a balancing of the discrepancies between the MD uniaxial predictions of the nonlinear theory and the observed MD uniaxial experimental data with the discrepancies between the CD uniaxial predictions of the nonlinear theory and the observed CD uniaxial experimental data. This may be expressed mathematically by equating the percent error between eq. (36) and the MD uniaxial prediction of the nonlinear theory when using the compromise function derivative with the percent error between eq. (37) and the CD uniaxial prediction of the nonlinear theory when using the compromise function derivative. Using eqs. (15,18,24,26,36,37,40,41), the balancing of percent errors condition described above can be expressed mathematically at a fixed level of effective strain e . This calculation leads to [24]

$$\left| \frac{W'_{comp}(e) - W'_{MD}(e)}{W'_{MD}(e)} \right| = \left| \frac{W'_{comp}(e) - W'_{CD}(e)}{W'_{CD}(e)} \right| \quad (42)$$

Rearrangement of eq. (42) yields a general closed-form expression for the compromise strain energy density function derivative

$$W'_{comp}(e) = \frac{2 W'_{MD}(e) W'_{CD}(e)}{W'_{MD}(e) + W'_{CD}(e)} \quad (43)$$

At a given moisture level, the compromise strain energy density function derivative can be seen to depend on a total of eight material constants by substituting eqs. (40,41) into eq. (43). These constants are the Poisson's ratios ν_{12} and ν_{21} , and the six hyperbolic tangent regression coefficients C_1^{MD} , C_2^{MD} , C_3^{MD} , C_1^{CD} , C_2^{CD} , C_3^{CD} .

The strain energy function itself could be obtained by integrating eq. (43). However, this calculation is not necessary since only $W'(e)$ appears in the stress-strain relations in eqs. (9).

The compromise strain energy function derivative has been evaluated at several moisture levels for the paper material under consideration in this work. These calculations were performed using eq. (43) and the regression constants tabulated in Figure 7 and the Poisson's ratios tabulated in Figure 12. Plots of the compromise strain energy function derivative at seven moisture levels are given in Figure 19. Also included in these graphs are plots of the functions $W'_{MD}(e)$ and $W'_{CD}(e)$. A combined plot of the compromise strain energy function derivative versus e at all of the different moisture levels is shown in Figure 20.

The compromise approach described above was chosen to achieve a balance between the accuracies of the MD and CD uniaxial predictions of the nonlinear theory. In Figure 21, the uniaxial MD and CD predictions of the nonlinear constitutive theory using the compromise strain energy density function derivative are correlated with the paperboard experimental stress-strain data from Figure 9 at seven different moisture levels. The theoretical curves were generated using eqs. (15,24) and the strain energy function derivatives calculated with eq. (43). The input data for these calculations were taken from the tables in Figure 7 and Figure 12. The nonlinear theory predictions are represented by the thick lines in Figure 21. They do not match the experimental data quite as well as the hyperbolic tangent empirical fits shown in Figure 8. However, the nonlinear constitutive model has the advantage of being able to predict response in biaxial stress states.

Constant C

The final input property needed for the nonlinear theory is the material constant C present in the shear stress-strain relation found in the third of eqs. (9). This constant can be evaluated at particular moisture levels using eq. (33) and the measured values of the initial shear modulus G_{12} and the strain energy function derivative $W'(0)$ at zero strain. The general expression for constant C in eq. (33) can be further specified by substitution of the compromise strain energy density function in eq. (43). This calculation yields

$$C = \frac{G_{12} [W'_{MD}(0) + W'_{CD}(0)]}{W'_{MD}(0) W'_{CD}(0)} \quad (44)$$

If the expressions for the MD and CD strain energy density function derivatives in eqs. (40,41) are evaluated at $e = 0$ and then substituted into eq. (44), the following expression for constant C is found

$$C = \frac{2G_{12}(1 - \nu_{12}\nu_{21})[\nu_{21}(C_1^{MD} + C_2^{MD}C_3^{MD}) + \nu_{12}(C_1^{CD} + C_2^{CD}C_3^{CD})]}{\nu_{12}\nu_{21}(C_1^{MD} + C_2^{MD}C_3^{MD})(C_1^{CD} + C_2^{CD}C_3^{CD})} \quad (45)$$

In this relation, constant C has been expressed in terms of the initial shear modulus G_{12} , the Poisson's ratios ν_{12} and ν_{21} , and the six hyperbolic tangent regression coefficients $C_1^{MD}, C_2^{MD}, C_3^{MD}, C_1^{CD}, C_2^{CD}, C_3^{CD}$.

Material constant C has been evaluated at several moisture levels for the paper under consideration using eq. (45) and the experimental data tabulated in Figures 7, 12, and 17. The results of these calculations are tabulated in Figure 22 and plotted in Figure 23. A nearly linear variation with moisture content has been observed.

SUMMARY AND CONCLUSIONS

In this project, the effects of moisture on the mechanical behavior of paperboard has been investigated. In particular, experiments under controlled environmental conditions have been performed to determine the effects of moisture content on the MD and CD initial elastic moduli, the Poisson's ratios, the initial shear modulus, and the shapes of the MD and CD uniaxial stress-strain curves. Seven different moisture levels were considered. The variations of the initial elastic moduli, the Poisson's ratios, and the initial shear modulus with moisture content were found to be approximately linear. The Poisson's ratios dramatically increased with increasing moisture content. In fact, a value of ν_{12} exceeding .6 was measured at 95% RH. At all levels of moisture, a three parameter hyperbolic tangent model accurately fit the observed nonlinear stress-strain curves. The results of these material characterization experiments were then utilized to calculate the input parameters to a set of biaxial nonlinear elastic stress-strain relations for paperboard. The moisture dependence of the three material constants and of the strain energy density function derivative utilized within the nonlinear model have been determined. The nonlinear model will be used in future studies to predict nonlinear elastic behavior of paperboard in biaxial stress situations at various moisture contents.

ACKNOWLEDGEMENTS

This research was supported by the U. S. D. A. Forest Products Laboratory, Madison, WI, and the Auburn University Pulp and Paper Research and Education Center.

REFERENCES

- Perkins, R. W., "Models for Describing the Elastic, Viscoelastic, and Inelastic Mechanical Behavior of Paper and Board," in Handbook of Physical and Mechanical Testing of Paper and Paperboard, Edited by R. E. Mark, Marcel Dekker, pp. 23-75 (1983).
- Suhling J. C., "Continuum Models for the Mechanical Response of Paper and Paper Composites: Past, Present, and Future," in Material Interactions Relevant to the Pulp, Paper, and Wood Industries, Vol. 197, Edited by D. F. Caulfield, J. D. Passaretti and S. F. Sobczynski, Materials Research Society, pp. 245-255 (1990).
- Thorpe, J. L., TAPPI, "Paper as an Orthotropic Thin Plate," 64 (3): 119-121 (1981).
- Petit, P. H. and Waddoups, M. E., Journal of Composite Materials, "A Method of Predicting the Nonlinear Behavior of Laminated Composites," 3 (1): 2-19 (1969).
- Sandhu, R. S., Journal of Aircraft, "Nonlinear Behavior of Unidirectional and Angle Ply Laminates," 13 (2): 104-111 (1976).
- Ramasubramanian, M. K. and Ko, Y. C., "Relationship Between the In-Plane Paper Properties and the Ball Burst Strength," in Mechanics of Cellulosic and Polymeric Materials, Edited by R. W. Perkins, ASME, AMD-Vol. 99, pp. 105-111 (1989).
- Paetow, R. and Gottsching, L., "The Two-Dimensional Nonlinear Elastic Material Law for Paper," Presented at the 1990 Progress in Paper Physics Seminar, Kalamazoo, MI, September 30 - October 3, 1990.
- Fung, Y. C. Foundations of Solid Mechanics, Prentice-Hall, 1965.
- Hahn, H. T. and Tsai, S. W., Journal of Composite Materials, "Nonlinear Elastic Behavior of Unidirectional Composite Laminates," 7 (1): 102-118 (1973).
- Pindera, M. J. and Herakovich, C. T., Journal of Applied Mechanics, "An Elastic Potential for the Nonlinear Response of Unidirectional Graphite Composites," 51 (3): 546-550 (1984).
- Luo, S. Y. and Chou, T. W., Journal of Applied Mechanics, "Finite Deformation and Nonlinear Elastic Behavior of Flexible Composites," 55 (1): 149-155 (1988).
- Suhling, J. C., Johnson, M. W., Rowlands, R. E. and Gunderson, D. E., "Nonlinear Elastic Constitutive Relations for Cellulosic Materials," in Mechanics of Cellulosic and Polymeric Materials, Edited by R. W. Perkins, ASME, AMD-Vol. 99, pp. 1-13 (1989).
- Johnson, M. W. and Urbanik, T. J., Journal of Applied Mechanics, "A Nonlinear Theory for Elastic Plates with Applications to Characterizing Paper Properties," 51 (1): 146-152 (1984).
- Lin, S. T. and Suhling, J. C., "Supercomputer Analysis of Paperboard Structures," in Mechanics of Cellulosic and Polymeric Materials, Edited by R. W. Perkins, ASME, AMD-Vol. 99, pp. 113-123 (1989).
- Lin, S. T., Suhling, J. C., Johnson, M. W. and Rowlands, R. E., "A Combined Analytical-Experimental-Numerical Analysis of the Burst Test for Paperboard Strength," in Mechanics of Wood and Paper Materials, Edited by R. W. Perkins, ASME, AMD-Vol. 112, pp. 71-84, (1990).

16. Gunderson, D. E., APPITA, "Edgewise Compression of Paperboard: A New Concept of Lateral Support," 37 (2): 137-141, (1983).
17. Andersson, O. and Berkyto, E., Svensk Papperstidning, "Some Factors Affecting the Stress-Strain Characteristics of Paper," 54 (13): 437-444 (1951).
18. Nissan, A. H., "Water Effects on Young's Modulus of H-Bonded Solids," in Fiber-Water Interactions in Papermaking, Edited by F. Bolam, Technical Section of the B.P. & B.M.A., pp. 609-629 (1978).
19. Brecht, W. and Wanka, R., Das Papier, "Contraction of Paper in the Cross Direction," 17 (4): 141-147 (1963).
20. Gottsching, L. and Baumgarten, H. L., "Triaxial Deformation of Paper under Tensile Load," in The Fundamental Properties of Paper Related to its Uses, Edited by F. Bolam, Technical Section of the B.P. & B.M.A., pp. 227-249 (1976).
21. Baum, G. A., Brennan, D. C. and Habeger, C. C., TAPPI, "Orthotropic Elastic Constants of Paper," 64 (8): 97-101 (1981).
22. Setterholm, V. C., Benson, R. and Kuenzi, E. W., TAPPI, "Method for Measuring Edgewise Shear Properties of Paper," 51 (5): 196-202 (1968).
23. Yeh, K. C., Considine, J. M. and Suhling, J. C., "Effects of Moisture on the Shear Behavior of Wood-Based Composites," in Mechanics of Wood and Paper Materials, Edited by R. W. Perkins, ASME, AMD-Vol. 112, pp. 193-200 (1990).
24. Yeh, K. C., The Effects of Moisture on the Mechanical Behavior of Nonlinear Orthotropic Media, Ph.D. Dissertation, Auburn University, 1991.

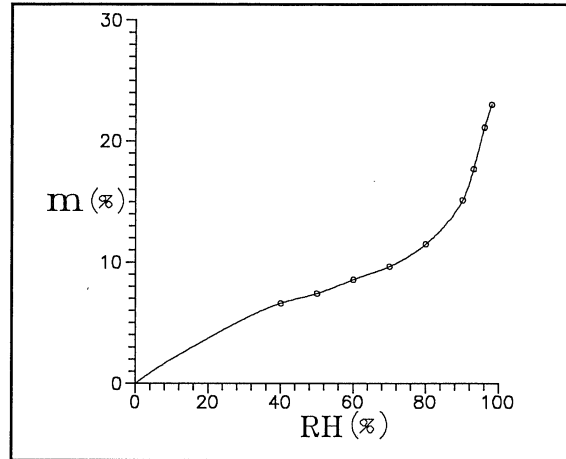


Figure 2 - Characteristic Adsorption Curve

RH (%)	m (%)
40	6.63
50	7.42
60	8.56
70	9.65
80	11.51
90	15.14
93	17.70
96	21.15
98	23.04

Figure 3 - Tabulated Values of Moisture Content Versus Relative Humidity

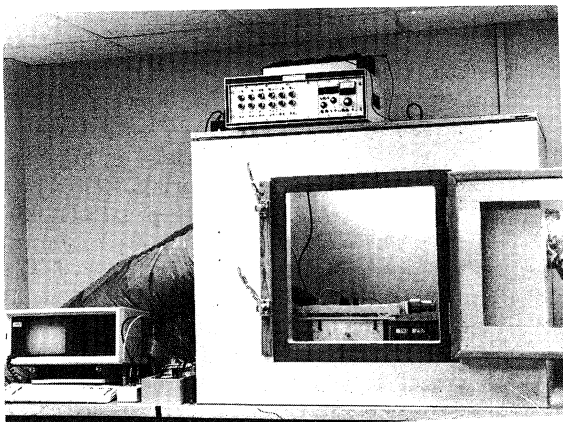


Figure 1 - Environmental Chamber

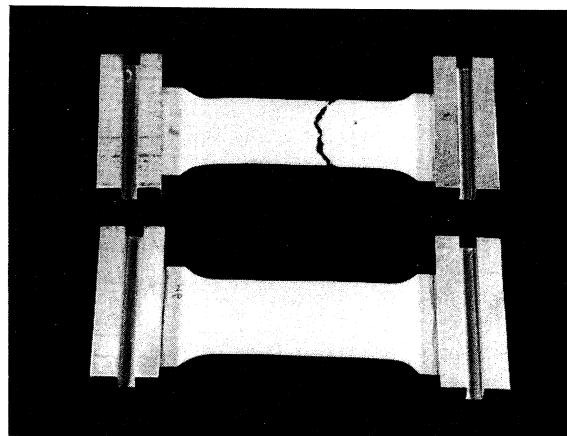


Figure 4 - Uniaxial Specimen Assemblies Before and After Testing

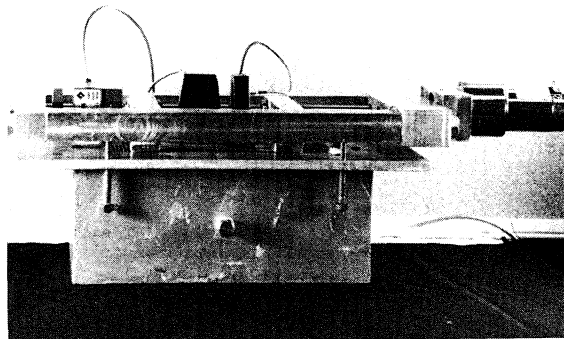


Figure 5 - Uniaxial Testing Unit

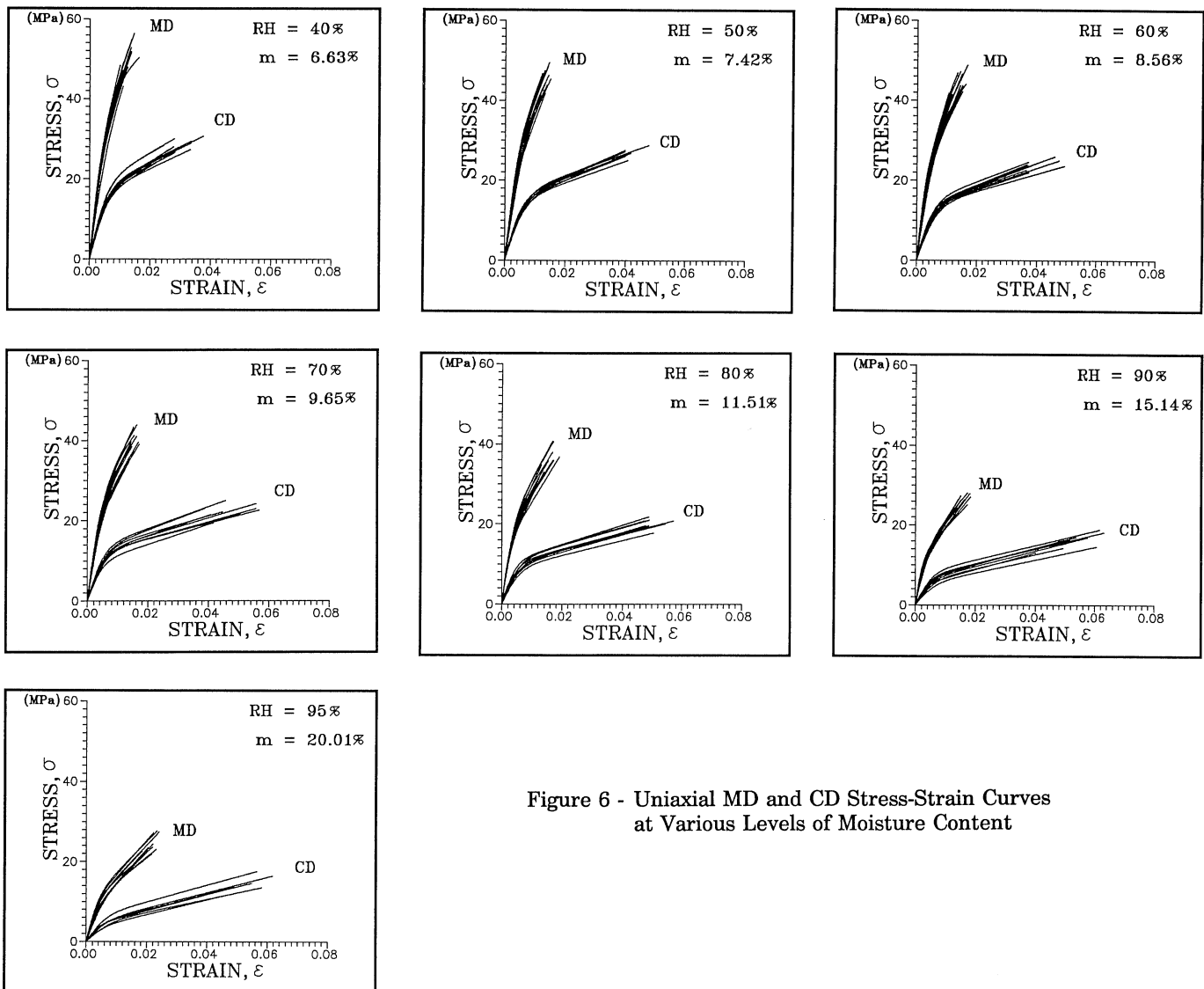


Figure 6 - Uniaxial MD and CD Stress-Strain Curves at Various Levels of Moisture Content

RH (%)	m (%)	C_1^{MD} (MPa)	C_2^{MD}	C_3^{MD} (MPa)	C_1^{CD} (MPa)	C_2^{CD}	C_3^{CD} (MPa)
40	6.63	25.49	203.9	1910	16.57	165.2	377.6
50	7.42	21.26	230.2	1851	14.47	170.0	302.6
60	8.56	23.12	207.4	1490	13.79	171.0	245.2
70	9.65	19.92	231.3	1378	12.25	160.2	205.2
80	11.51	16.20	253.8	1240	9.80	174.0	203.1
90	15.14	10.96	281.8	967	5.87	184.0	190.8
95	20.01	7.37	245.1	797	4.05	173.5	196.0

Figure 7 - Calculated Hyperbolic Tangent Regression Coefficients at Various Levels of Moisture Content

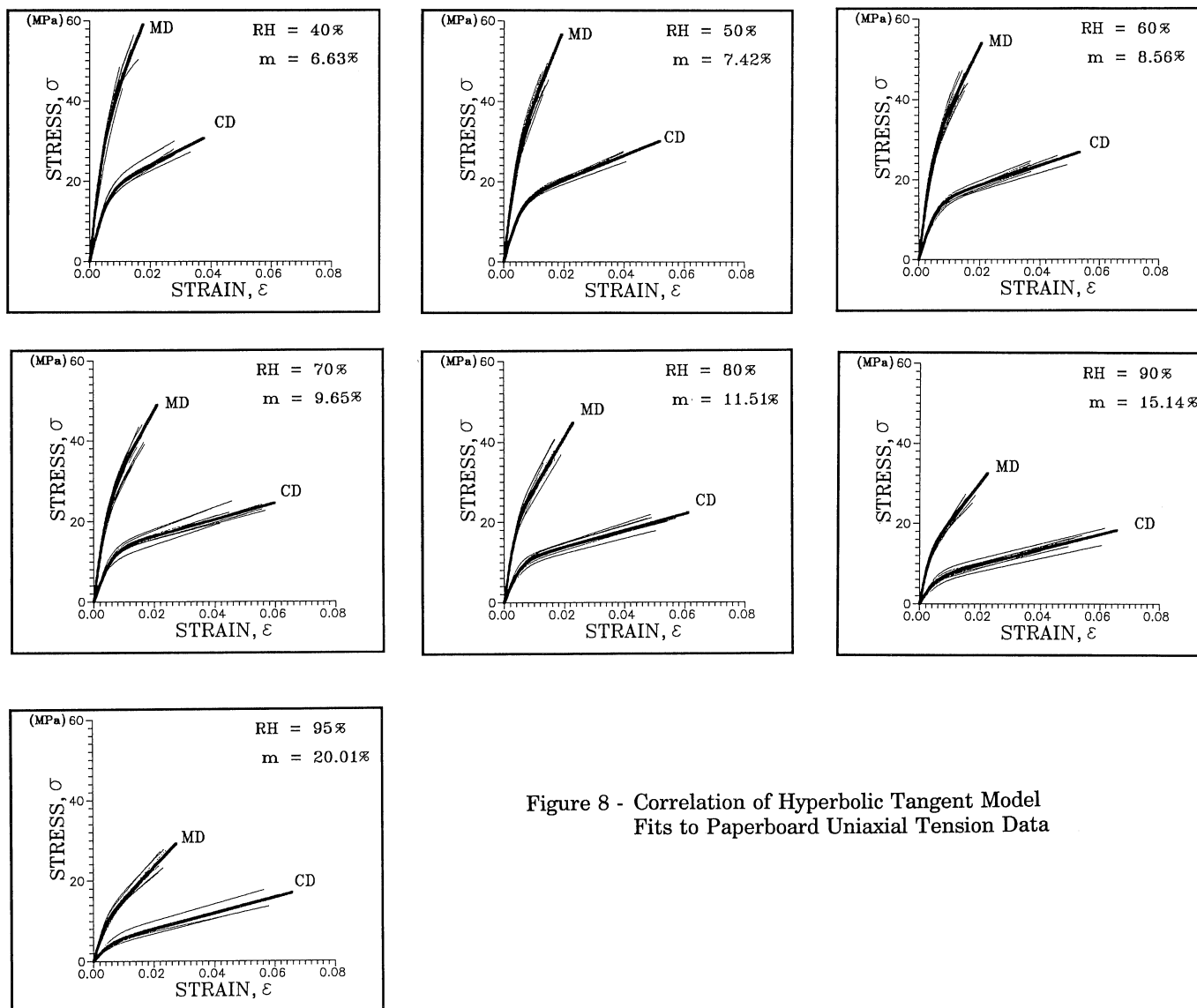


Figure 8 - Correlation of Hyperbolic Tangent Model Fits to Paperboard Uniaxial Tension Data

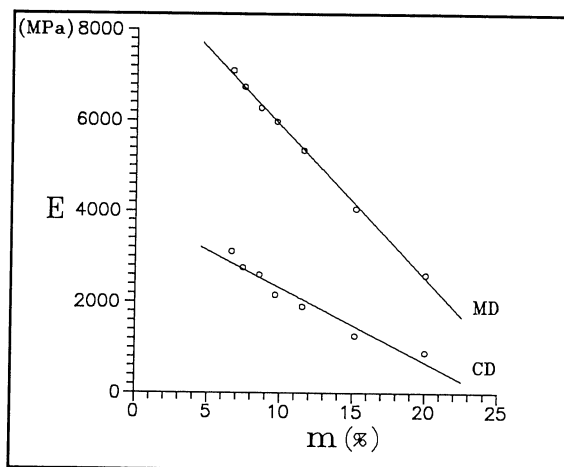


Figure 9 - Elastic Moduli Versus Moisture Content

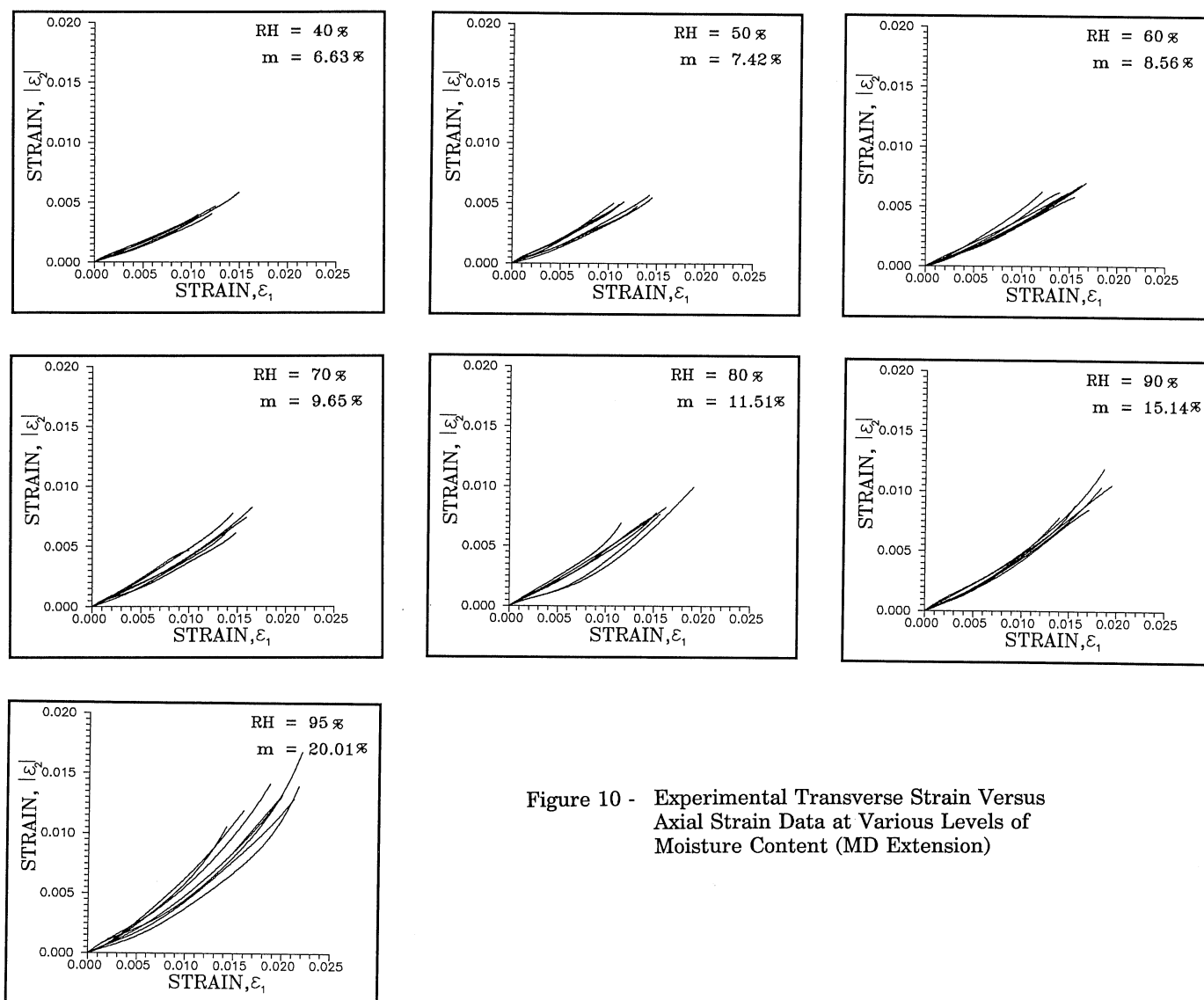


Figure 10 - Experimental Transverse Strain Versus Axial Strain Data at Various Levels of Moisture Content (MD Extension)

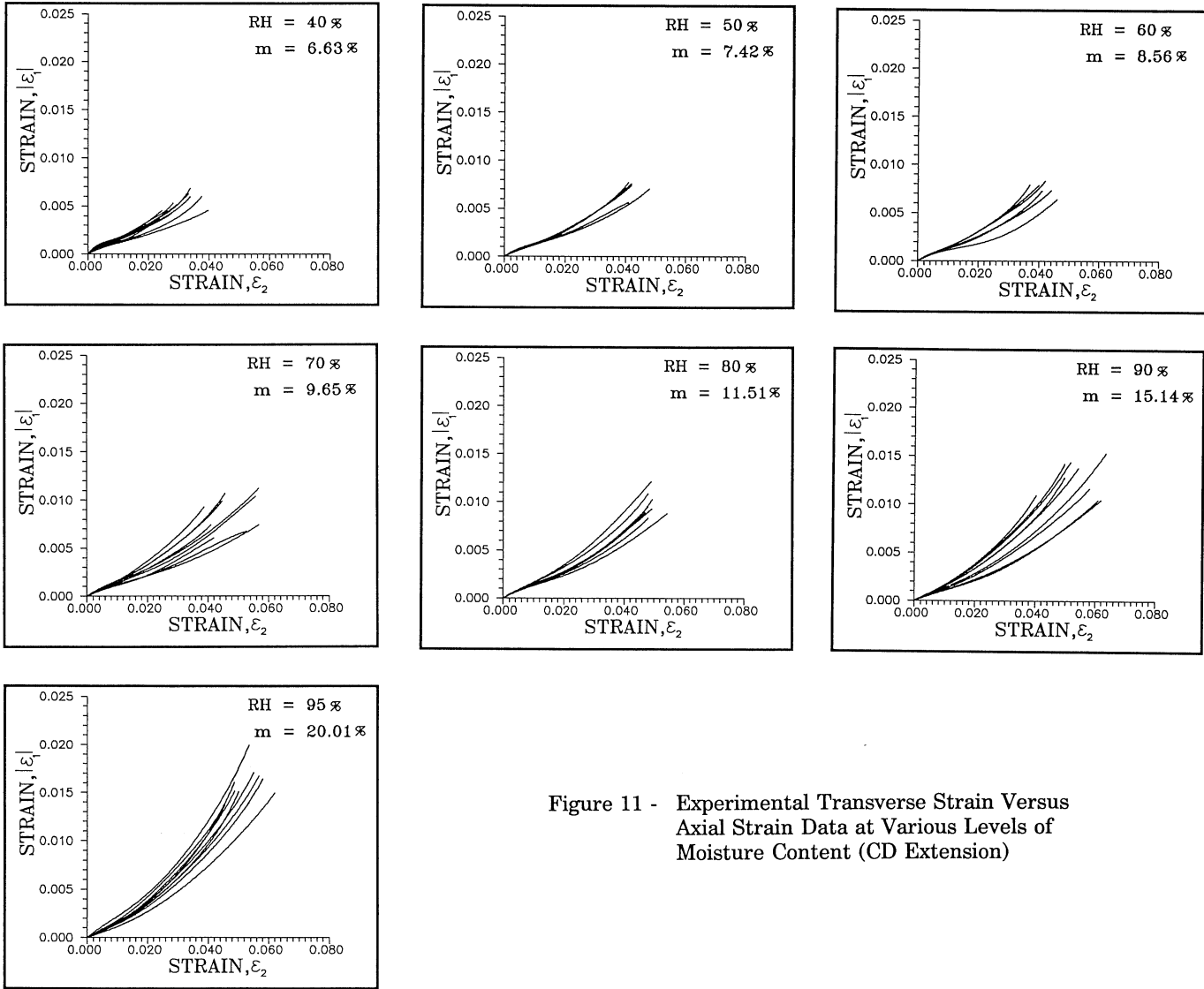


Figure 11 - Experimental Transverse Strain Versus Axial Strain Data at Various Levels of Moisture Content (CD Extension)

RH (%)	m (%)	ν_{12}	ν_{21}	$\nu_{12,initial}$	$\nu_{21,initial}$
40	6.63	0.355	0.141	0.367	0.220
50	7.42	0.387	0.157	0.385	0.197
60	8.56	0.420	0.167	0.395	0.214
70	9.65	0.456	0.172	0.424	0.200
80	11.51	0.488	0.187	0.428	0.200
90	15.14	0.554	0.217	0.399	0.180
95	20.01	0.641	0.285	0.413	0.182

Figure 12 - Tabulated Values of the Poisson's Ratios Versus Moisture Content

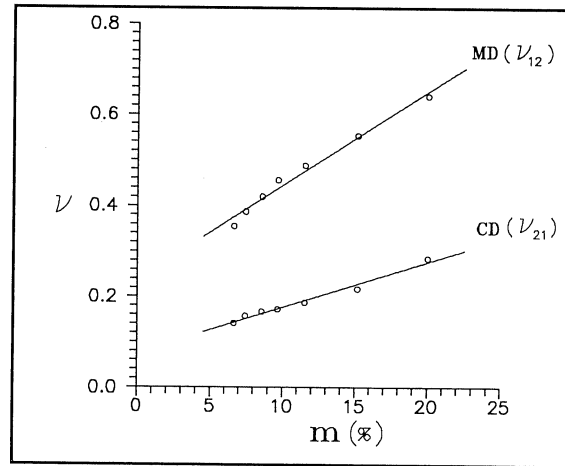


Figure 13 - Poisson's Ratios Versus Moisture Content

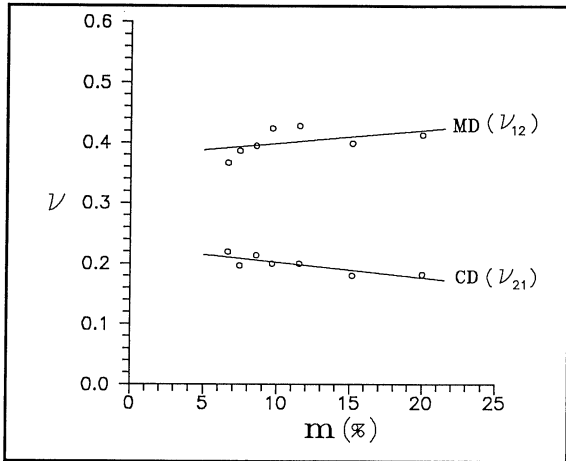


Figure 14 - Initial Poisson's Ratios Versus Moisture Content

RH (%)	m (%)	G_{12} (MPa)
16	2.10	2503
30	5.00	2212
40	6.63	1912
50	7.42	1734
60	8.56	1644
70	9.65	1560
80	11.51	1123
90	15.14	671
95	20.01	446

Figure 17 - Tabulated Values of the Shear Modulus Versus Moisture Content

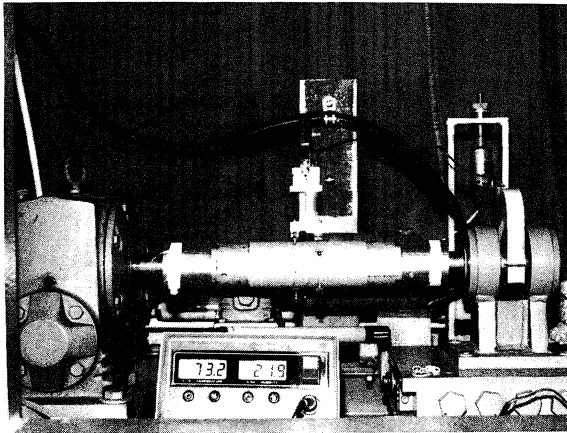


Figure 15 - Torsion Apparatus

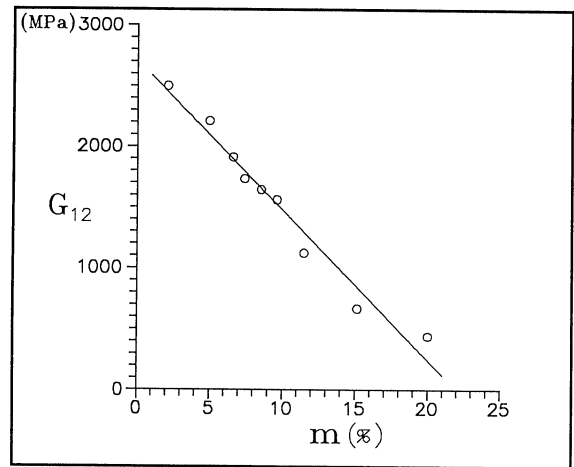


Figure 18 - Shear Modulus Versus Moisture Content

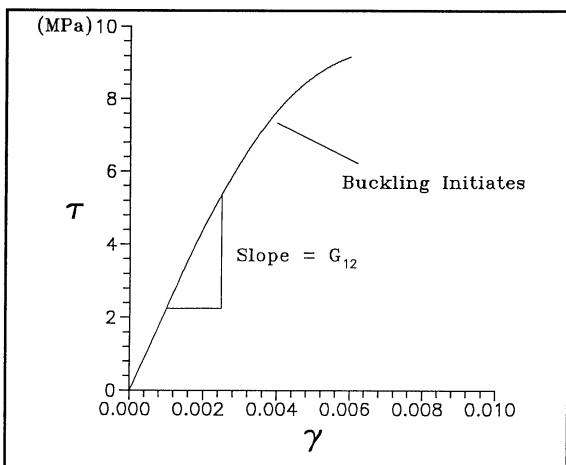


Figure 16 - Typical Measured Shear Stress-Strain Curve

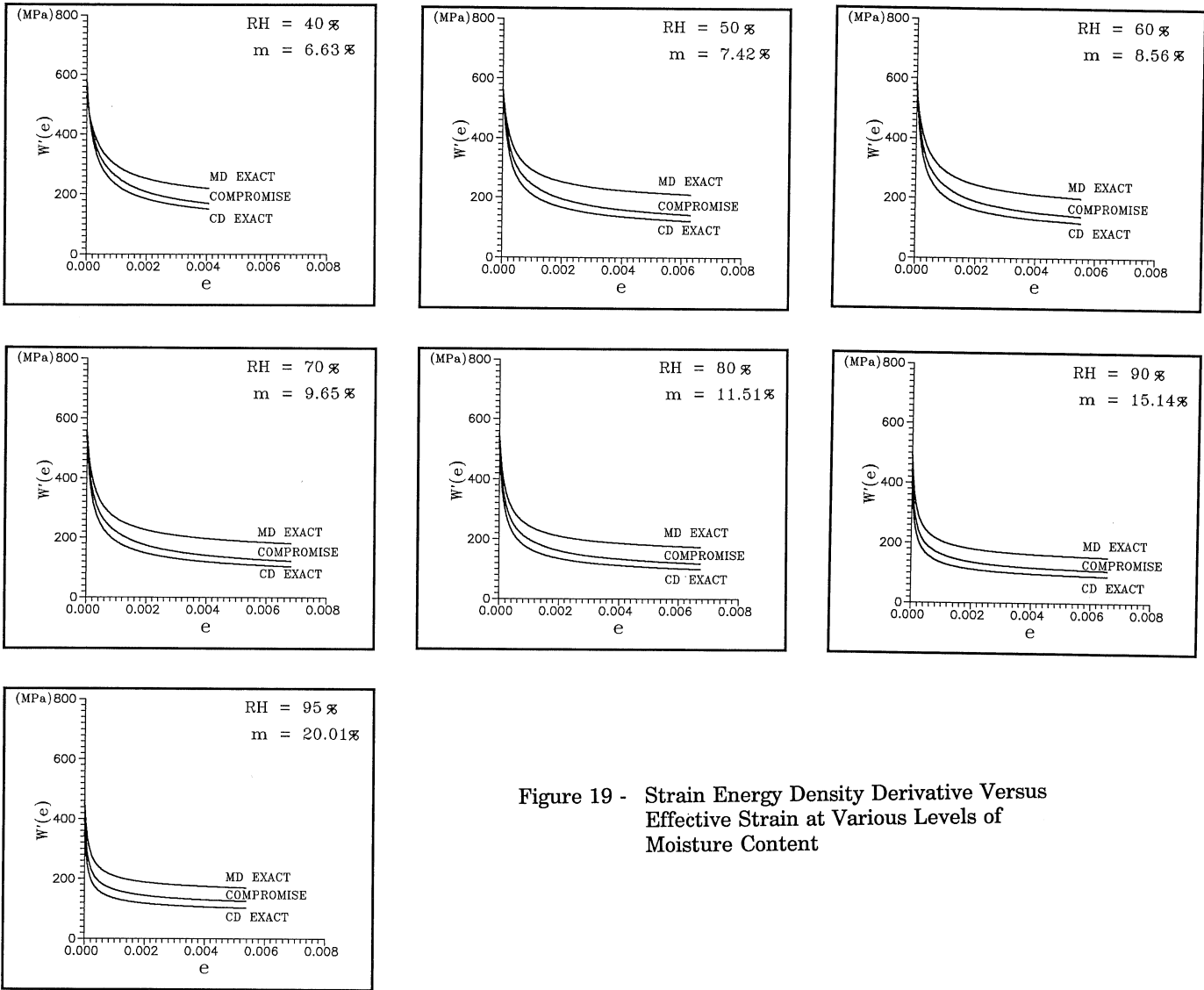


Figure 19 - Strain Energy Density Derivative Versus Effective Strain at Various Levels of Moisture Content

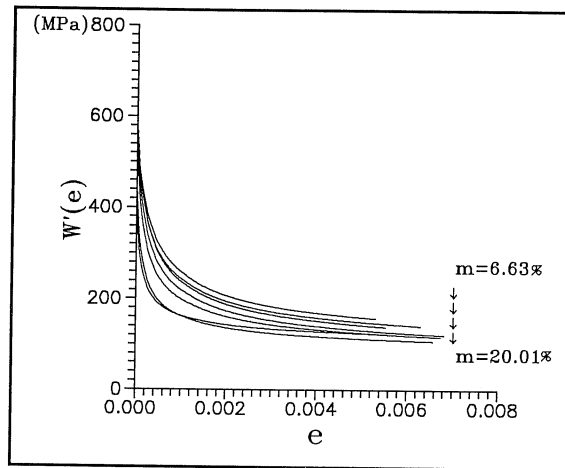


Figure 20 - Combined Plot of Strain Energy Density Derivative Versus Effective Strain

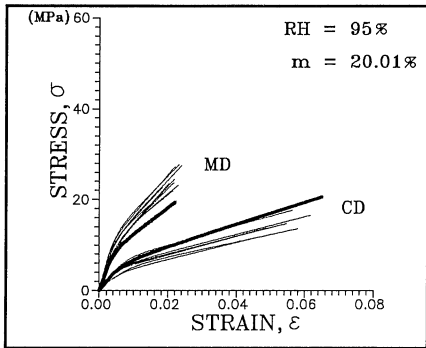
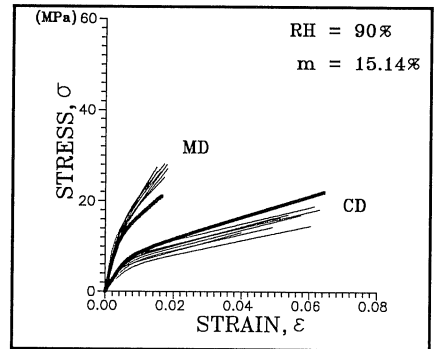
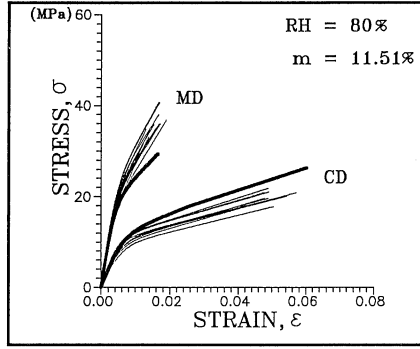
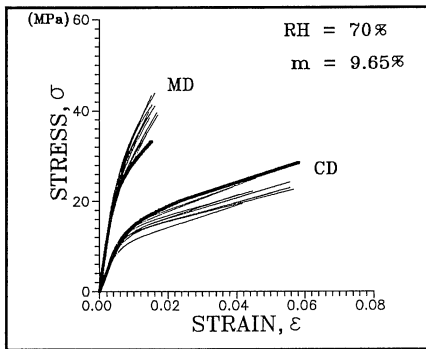
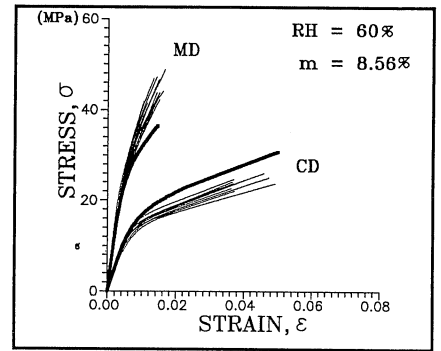
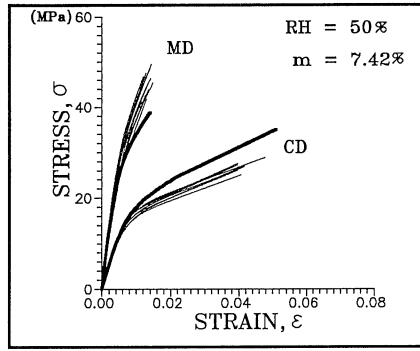
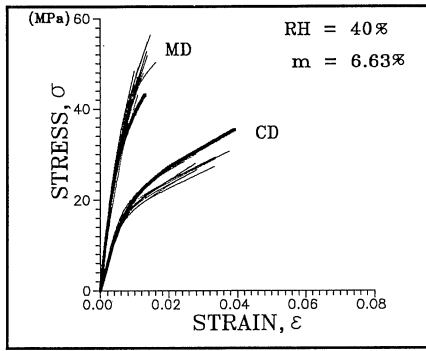


Figure 21 - Nonlinear Constitutive Theory Stress-Strain Curve Predictions and Paperboard Uniaxial Experimental Data

RH (%)	m (%)	C
40	6.63	6.91
50	7.42	6.12
60	8.56	5.71
70	9.65	5.70
80	11.51	4.23
90	15.14	3.02
95	20.01	2.25

Figure 22 - Tabulated Values of Material Constant C Versus Moisture Content

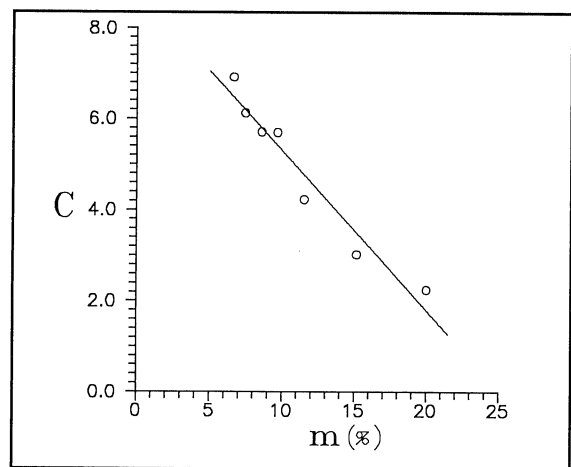


Figure 23 - Material Constant C Versus Moisture Content

